Proceedings of the Second International Workshop on
Fundamental Issues and Future Research Directions for Parallel Mechanisms and Manipulators
September 21–22, 2008, Montpellier, France
N. Andreff, O. Company, M. Gouttefarde, S. Krut and F. Pierrot, editors

Kinematic and Elastodynamic Design Optimisation of the 3-DOF Gantry-Tau Parallel Kinematic Manipulator

ILYA TYAPIN
School of Information Technology
and Electrical Engineering
University of Queensland
Brisbane, Queensland, Australia 4001
ilya@itee.uq.edu.au

GEIR HOVLAND
Department of Engineering
University of Agder
N-4898 Grimstad, Norway
Email: geir.hovland@uia.no

TORGNY BROGÅRDH
ABB Robotics
SE-721 68 Västerås, Sweden
Email: torgny.brogardh@se.abb.com

Abstract: *One of the main advantages of the Gantry-Tau machine is a large accessible workspace/footprint ratio compared to many other parallel machines. The Gantry-Tau improves this ratio by allowing a change of assembly mode without internal link collisions or collisions between the links and the moving* $\boldsymbol{TCP}$ *platform. However, the optimal kinematic, elastostatic and elastodynamic design parameters of the machine are still difficult to calculate and this paper introduces an optimisation scheme based on the geometric approach for the workspace area and the functional dependencies of the elements of the static matrix and the Laplace transform to define the first resonance frequency. The method to calculate the first resonance stiffness assumes that each link and universal joint can be described by a mass-spring-damper model and calculates the transfer function from a Cartesian force or torque to Cartesian position or orientation. These approaches are significantly faster than analytical methods based on the inverse kinematics or the general Finite Elements Method (FEM). Kinematic design obtained by optimisation according to this paper gives a workspace/footprint ratio of more than 2.7 and the first resonance frequency of more than 50 Hz with components of an existing lab prototype at the University of Agder.*

1 Introduction

A generalised parallel kinematic manipulator (PKM) is a closed-loop kinematic chain mechanism where the end-effector is linked to the base by several independent kinematic chains, Merlet (2000). It may consist of redundant mechanisms with more actuators than the number of controlled degrees of freedom of the end-effector. The study of PKMs has been an active research field in robotics and mechanical design for a long time. From the first ideas of Gough (1957) and Stewart (1965), many mechanisms and design methods have been developed. The concept of using the parallel mechanism as a spatial motion mechanism with 6-DOFs (degree of freedom) was first presented by Gough (1957). Stewart proposed a 6-DOFs platform targeting the flight simulator application. In the late 1980s a new field of applications and research was developed by Clavel (1988). The Delta robot presented by Clavel was a base for a large range of machines dedicated to high-speed applications but because of small workspace in relation to footprint and limited number of degrees of freedom the robot can not be used as a general purpose manipulator. In contrast, Pierrot proposed a 6-DOF fully-parallel robot HEXA. The HEXA robot, Pierrot *et al.* (1992) and Uchiyama *et al.* (1990), is an extension of the DELTA mechanism having 6 DOFs but because the workspace/footprint ratio and tilting angles are small this robot has also a limited capability compared to serial manipulators. Due to the problems with small accessible workspace, relatively small tilting angles and in some cases wide ranging stiffness values inside the workspace the use of PKMs in industry is still limited.

The Tau family of PKMs was invented by ABB Robotics, see Brogårdh *et al.* (2000). The Gantry-Tau was designed to overcome the workspace limitations while retaining many advantages of PKMs such as low moving mass, high stiffness and no link twisting or bending moments. For a given Cartesian position of the robot each arm has two solutions for the inverse kinematics, referred to as the left- and right-handed configurations. While

operating the Gantry-Tau in both left- and right-handed configurations, the workspace will be significantly larger in comparison with both a serial Gantry-type robot and other PKMs with the same footprint and with only axial forces in the links of the arms. The intended application of the robot is for machining operations requiring a workspace equal to or larger than of a typical serial-type robot, but with higher stiffness. However, the robot can also be designed for very fast material handling and assembly or for high precision processes such as laser cutting, water jet cutting and measurement.

Currently, there exist large gaps between the stiffness and dynamic properties of serial-type robots and many of the developed PKM prototypes. An industrial serial-type robot typically has a Cartesian stiffness in the range 1-2 Newtons per micron ($N/\mu m$) and resonance frequencies below 10 Hz. A high-speed machining centre typically has stiffness larger than $50N/\mu m$ and resonance frequencies larger than 50 Hz. Between these specifications there exists a large range of untapped application areas for PKMs. With higher stiffness and resonance frequencies compared to serial robots, PKMs can provide benefits such as reduced oscillations and overshoots which in turn can lead to economic benefits gained from reduced cycle-times.

In this paper the triangular-link variant of the 3-DOF Gantry-Tau structure is considered, which was first presented in Brogårdh *et al.* (2005). Triangular mounted links give several advantages: they enable a reconfiguration of the robot and a larger reach is obtained in the extremes of the workspace. When using parallel links, the orientation of the manipulated platform will be constant, which increases the risk of collisions of the arms with the manipulated platform in the extremes of the workspace area.

In Johannesson *et al.* (2004) a basic workspace optimisation method for the 3-DOF Gantry-Tau with no triangular links was presented. Two geometrical parameters of the machine were optimised to maximise the cross-sectional workspace area. Our paper is an extension of the work in Johannesson *et al.* (2004). The new contributions of this paper are: the optimisation is made for the Gantry-Tau with triangular mounted links, the optimisation is made over the whole workspace volume and not just the cross-sectional workspace area. The geometric approach for the Gantry-Tau reachable workspace area calculation was presented in Tyapin *et al.* (2007) for the first time and briefly presented in Section 3.

In order to calculate the workspace one can employ discretisation methods, geometrical methods or analytical methods. For the discretisation method a grid of nodes with position and orientation is defined. Then the kinematics is calculated for each node and it is straightforward to verify whether the kinematics can be solved and to check if joint limits are reached or link interference occurs. The discretisation algorithm is simple to implement but has some serious drawbacks. It is expensive in computation time and results are limited to the nodes of the grid. One example of this approach is Dashy *et al.* (2002).

Analytical workspace area methods which investigate the properties of the kinematic transmission are described in Angeles (1985), Goldenberg *et al.* (1985). Most approaches are based on the inverse kinematics because it can typically be solved in closed form and it is easer to distinguish between multiple solutions. Whereas discretisation methods are based on the full inverse kinematics, the analytic approaches usually only require parts of the inverse kinematics. Even so, analytical methods can be expensive in computation time.

Using geometrical methods the workspace can be calculated as an intersection of simple geometrical objects, Merlet (2000), for example spheres. The works presented in Chablat *et al.* (2003), Liu *et al.* (2000) and Tyapin *et al.* (2006) are examples of partial geometric approaches to calculate the workspace of a 3-DOF PKM. They are only partial geometric because numeric integration is used to calculate the workspace. Design optimisation was attempted by Chablat *et al.* (2003), Liu *et al.* (2000) and Tyapin *et al.* (2006). In addition, Liu *et al.* (2000) presented the relationships between the workspace and link lengths of all planar 3-DOF parallel manipulator. The workspace analysis and design optimisation of the parallel machine was also presented in Monsarrat *et al.* (2003). In Monsarrat *et al.* (2003) the workspace was defined by three rotational angles. In our paper the static matrix was presented by one platform rotational angle α.

Another interesting work is the paper by Kim *et al.* (1997). In that paper a fully geometric approach to calculate the reachable workspace was presented for a 6-DOF Hexapod type PKM. The differences compared to our paper are the use of variable link lengths instead of fixed actuators at the robot base and no design optimisation was attempted in Kim *et al.* (1997). The closest work to this paper was presented in Bonev *et al.* (2001) for the orientation workspace, but both Kim *et al.* (1997) and Bonev *et al.* (2001) use the inverse kinematics (rotational matrix) to define the workspace. Most researchers use a basic inverse kinematics (rotational matrix) or Jacobian matrix as a part of a geometric approach to define a workspace. However, in this paper a rotational matrix is used to define the static matrix.

A new and general approach for calculating the dynamic frequency response of parallel kinematic machines (PKMs) with six links (Hexapods) was presented in Hovland *et al.* (2007). This method exploits the fact that this type of PKMs only experiences axial link forces and the method is significantly faster than general Finite Element Method (FEM) used for other PKM structures which also take link bending and twisting moments into account. In this paper the results from Hovland *et al.* (2007) were further improved by introducing functional dependencies of the frequency response.

A frequency response model of a PKM over the entire working envelope is an essential tool when designing and dimensioning PKMs for high-speed machining and other applications. The flexibility of PKMs may cause structural resonance in the cutting process and mechanical interaction with the control system because of regenerative and modal chattering, which is the main concern in high-speed machining. Moreover, high structural resonance frequencies are needed to obtain a high bandwidth robot control. High bandwidth control means accurate and fast control of tool position, speed and force.

The majority of published works about PKM structures has been on kinematics and singularity analysis. The study of dynamics of PKMs has received less attention, and flexible dynamics less than rigid-body dynamics. One of the first published works on flexible PKM dynamics was presented by Fattah *et al.* (1995).

A 3-DOF spatial PKM with three flexible links was modelled and simulated. The model took both axial forces and bending moments into account. The model was only simulated in the time-domain, and no frequency response data was presented.

Two recent publications dealing with modelling of flexible PKMs were presented by Zhou *et al.* (2006) and Chen *et al.* (2006). Both papers modelled Tripod PKMs with flexible links. Because of the Tripod structure, the flexible dynamic models must take link bending and twisting moments as well as axial forces into account. Chen *et al.* (2006) presents a frequency response diagram of a Tripod and is able to quantify the lowest resonance frequency of the machine over the entire working envelope.

Very little work has been presented on flexible dynamic modelling of Hexapod PKMs. Xi *et al.* (2001) is an example of a publication of a rigid-body dynamics model of a Hexapod. To our knowledge no general flexible links dynamics models which exploit the Hexapod structure have previously been published, except for Hovland *et al.* (2007).

The main benefit of the work in this paper is the savings in computational effort. The method in this paper is more than 4 times faster than the method presented in Hovland *et al.* (2007). Also, in Hovland *et al.* (2007) the variations of link stiffness and mass as a functions of link length were ignored because of the joint stiffness are being much lower than the link stiffness. In this paper the link stiffness values as functions of the link lengths were taken into account and link stiffness were found for each link. As a result, the method presented in this paper is more accurate and faster. The time saving is possible because the static matrix and Jacobian matrices for the Laplace transform will be found from a functional dependency, where the coefficients of the function have been found analytically. In addition, the workspace will be discretised in one axis only. In the work Hovland *et al.* (2007) the static matrix had to be recalculated for every point of the workspace and for a different frequencies ω of the Laplace function.

Brief descriptions of the kinematics and workspace volume functions are presented in sections 2 and 3. The statics and dynamics are explained in sections 4 and 5. The first resonance frequency calculation method based on the Laplace transform is presented in section 6. The combined optimisation problem is formulated in section 7. The results are shown in section 8 and finally the conclusions are presented in section 9.

2 Kinematic Description

In this paper we consider the triangular-link version of the Gantry-Tau structure with no telescopic links, which is illustrated in Fig. 1 and Fig. 2.

The 3-DOF Gantry-Tau can be manually reconfigured while the 5-DOF version, see Hovland *et al.* (2008), can be automatically reconfigured while avoiding singularities. The architecture consists of a fixed base and a mobile platform connected by three legs. Fig. 1 shows the PKM structure in both the left-handed and right-handed configuration (also called assembly or working modes). As for the basic Gantry-Tau structure, the position of one end of each of the three parallel arms (lengths L_1, L_2 and L_3) is controlled by a linear actuator with actuation variables q_1, q_2 and q_3, see Fig. 2. L_i are the arm lengths according to Fig. 1. The actuators are aligned in the direction of the global X coordinate. The arm connected to actuator q_1 consists of one single link. The arm connected to actuator q_2 consists of two parallel links. The arm connected to actuator q_3 consists of three links, where two links are mounted in a triangular configuration. The structure and kinematics of the Gantry-Tau have been presented before, for example in Brogårdh *et al.* (2005), Murray *et al.* (2005) and Williams *et al.* (2006). The actuator track locations are fixed in the Y and Z directions and the locations are denoted T_{1y}, T_{1z}, T_{2y}, T_{2z}, T_{3y} and T_{3z}, respectively. The dimensioning of the PKMs support frame in the case it is symmetric is given by the two variables Q_1 and Q_2 as illustrated in Fig. 1, where Q_1 is the depth and Q_2 is the height. The width of the machine in the X direction is given by the length of the actuators.

Fig. 3 shows the manipulated platform and the fixed kinematic parameters of the moving platform, which are not included in the design optimisation. The points A, B, C, D, E and F are the link connection points. The arm with one single link connects the actuator q_1 with platform point F. The arm with two links connects actuator q_2 with the platform points A and B. The arm with three links connects actuator q_3 with the platform points C, D and E. The triangular pair is connected to points C and E.

The prototype of the 3-DOF Gantry-Tau with a triangular-mounted link pair built at the University of Agder (Norway) is shown in Fig. 2.

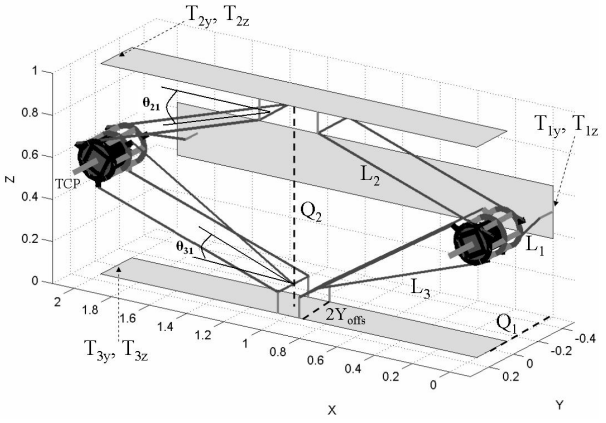

Figure 1: The 3-DOF reconfigurable Gantry-Tau robot.

3 Workspace

A fully geometric approach to define the reachable workspace areas of the Gantry-Tau is summarised in this section and was published before in Tyapin *et al.* (2007). In addition, the whole workspace volume calculation method is used as a summation of the workspace areas for the given X coordinates.

The benefit of a geometric approach is that it is much faster and more accurate than numerical solutions based on manipulator kinematics. In addition, the geometric approach developed in this paper also handles the fact that the platform orientation is not constant. Care must be taken to avoid collisions between the

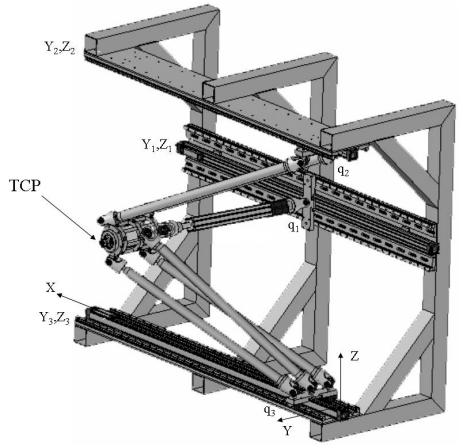

Figure 2: Prototype of a 3-DOF Gantry-Tau with a triangular-mounted link pair.

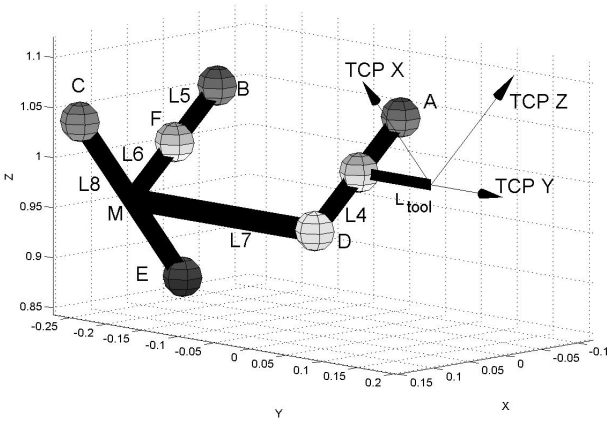

Figure 3: The manipulated platform of the Gantry-Tau robot.

arms, platforms and actuators, see Hovland *et al.* (2007). Fig. 4 shows three circles, one for each arm. The centres of the circles are located at the actuator positions. The radii of the circles equal the arm lengths plus the distance from the end of the arm to the **TCP**. The **TCP** can only reach points inside all of the circles. Fig. 4 also contains three solid lines in the YZ-plane. The **TCP** is not allowed to move outside these lines because they indicate the positions of the support framework. Note that it is possible to get outside these lines at positions where the links and platform do not collide with the linear actuators, for example at $Y > 0.2$ and with a small platform also with Y about -0.3. However, these areas are omitted in the analysis in this paper.

The valid **TCP** positions are illustrated in the grey area in Fig. 4. This area (A_{total}) can be calculated as a sum of subareas according to:

$$A_{total} = A_1 + A_2 + A_3 + A_4 \quad (1)$$

The subareas are in turn calculated by smaller areas as exemplified for the area A_3 in Fig. 5. The subarea A_3 consists of two segments of a circle for small values of Q_2 because the upper limit of the workspace is partly circular and partly straight line. The first segment of a circle is a segment between points

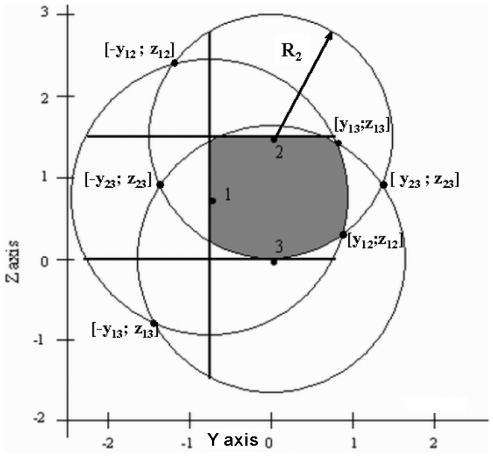

Figure 4: *The cross-sectional workspace area of the Gantry-Tau in the YZ-plane.*

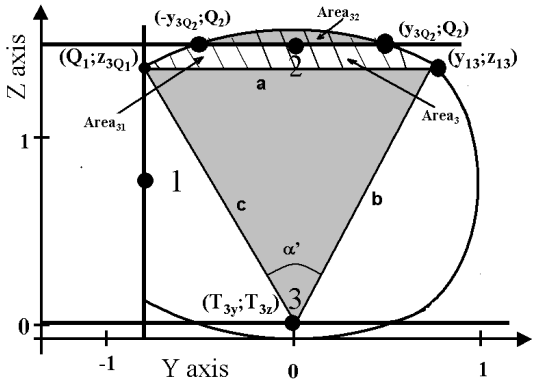

Figure 5: *Illustration of workspace Area 3.*

$(Q_1; z_{3Q_1})$, $(y_{13}; z_{13})$ and a centre is in the third arm actuator position $(T_{3y}; T_{3z})$. The point $(y_{13}; z_{13})$ is a cross point between two circles. The centres and radii of the circles are arm lengths and actuator positions for the arms 1 and 3, see Fig. 4. The point $(Q_1; z_{3Q_1})$ is a cross point between the support frame limit Q_1 and the third arm circle. The second segment of a circle has two limits $(-y_{3Q_2}; Q_2)$, $(y_{3Q_2}; Q_2)$ and a centre in the third arm actuator position. The limits are cross points between the support frame limit Q_2 and the third arm circle. At the bigger values of Q_2 the upper limit will be the circle arc between the points $(Q_1; z_{3Q_1})$ and $(y_{13}; z_{13})$.

When the expressions for the cross sectional areas have been obtained the next step is to calculate the workspace volume as a function of the cross-sectional areas. The geometric shape of the workspace volume is very difficult to describe as a whole or several geometrical shapes. Fig. 6 shows the workspace in the XZ-plane, which can be divided into 3 sections, sections 1 and 3 outside the guide ways and section 2 between the guide ways. The workspace volume calculation consists of a several steps. Firstly, the upper and lower bounds x_1 and x_4 for **TCP** on the X-axis must be found, and following this, additional bounds x_2 and x_3, that depend on the kinematics must be determined. These additional bounds are the actuator limits $x_2 = X_L$ and $x_3 = X_U$,

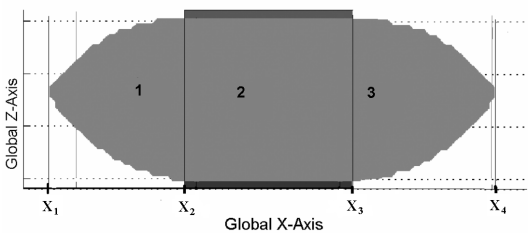

Figure 6: *The workspace area of Gantry-Tau machine in the XZ-plane when it is reconfigured to work in both positive and negative x-direction.*

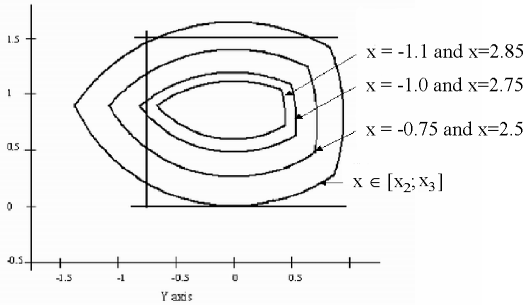

Figure 7: *The change of the workspace of the Gantry-Tau robot in the YZ-plane as a function of x.*

illustrated in Fig. 6. Following this, new radii for the three circles have to be found, one for each arm. The new radii depend on the given x position. Finally, the cross-sectional workspace area can be calculated. Some different workspace areas for the given x positions are presented in Fig. 7

The 4 bounds x_1, x_2, x_3, x_4 define 3 sections on the global X-axis. The sections are $[x_1x_2], [x_2x_3], [x_3x_4]$. These 3 sections are numbered in Fig. 6. The $\mathbf{TCP}$ can only reach points with x-coordinates between x_1 and x_4. Between these limits, the cross-sectional area varies as illustrated in Fig. 7.

The radii for the three circles in Fig. 4 depend on the x-coordinate. For the section $x \in [x_1x_2]$, see Fig. 7 the radii are defined as follows.

$$L_1^{'} = \sqrt{L_1^{''} - (x - x_2)^2} \quad L_2^{'} = \sqrt{L_2^{''} - (x - x_2)^2} \tag{2}$$

$$L_{3d}^{'} = \sqrt{L_3^{''} - (x - x_2)^2} \tag{3}$$

where the original arm lengths plus the distances from the ends of the arms to the $\mathbf{TCP}$ are denoted $L_1^{''}$,$L_2^{''}$, $L_3^{''}$.

The workspace volumes for the sections $x \in [x_1x_2]$ and $x \in [x_3x_4]$ are the same and do not have to be computed numerically twice. In the section $x \in [x_2x_3]$ the radii equal the nominal values, ie.

$$L_1^{'} = L_1^{''} \quad L_2^{'} = L_2^{''} \quad L_{3d}^{'} = L_3^{''} \tag{4}$$

The volume function is calculated partially numerically as described below.

$$V_R = 2 * \sum_{x=x_1}^{x=x_2} A_{Total}(x)\delta + A_{Total}(x_2) * [x_2x_3] \tag{5}$$

where δ is a step of the summation and $A_{Total}(x)$ is a workspace area for the given x-coordinate, V_R is a volume of the reachable workspace.

4 Static Analysis

This section contains equations and matrices which are required for the dynamic analysis in section 5.

$$\mathbf{X} = [X\ Y\ Z]^T \qquad \theta = [\alpha\ \beta\ \gamma]^T$$
$$\mathbf{F} = [F_x\ F_y\ F_z]^T \qquad \mathbf{M} = [M_x\ M_y\ M_z]^T$$
$$\mathbf{L} = [l_1\ l_2\ l_3\ l_4\ l_5\ l_6]^T \qquad \mathbf{F}_a = [F_1\ F_2\ F_3\ F_4\ F_5\ F_6]^T$$

where X, Y, Z are the Cartesian $\mathbf{TCP}$ coordinates, α, β, γ are the Cartesian $\mathbf{TCP}$ orientation angles, l_i are the link lengths and F_i are link forces where $i = 1, \cdots, 6$. F_x, F_y and F_z are the external Cartesian forces acting on the $\mathbf{TCP}$ and M_x, M_y and M_z are the external Cartesian torques acting on the $\mathbf{TCP}$. The relationship between the $\mathbf{TCP}$ forces and the link forces are.

$$\mathbf{F} = \sum_{i=1}^{6} F_i\mathbf{u}_i \qquad \mathbf{M} = \sum_{i=1}^{6} F_i\mathbf{A}_i \times \mathbf{u}_i \tag{6}$$

where $\mathbf{u_i}$ is a unit vector in the direction of link i and $\mathbf{A_i}$ is a vector pointing from the $\mathbf{TCP}$ to the end-point of link i on the platform. The two equations above can be rewritten using the 6×6 statics matrix $\mathbf{H}$.

$$\begin{bmatrix} \mathbf{F} \\ \mathbf{M} \end{bmatrix} = \mathbf{H}\mathbf{F}_a \qquad \begin{bmatrix} \mathbf{\Delta X} \\ \mathbf{\Delta}\theta \end{bmatrix} = \mathbf{J}\mathbf{\Delta L} \tag{7}$$

The Jacobian matrix of the PKM relates changes in Cartesian position $\mathbf{\Delta X}$ and orientation $\mathbf{\Delta}\theta$ with changes in the link lengths $\mathbf{\Delta L}$ as shown in eq.(7) (right). Gosselin (1990) showed the duality between the statics and the link Jacobian for PKMs, ie.

$$\mathbf{H}^{-1} = \mathbf{J}^T \tag{8}$$

Based on the duality result, the Cartesian stiffness matrix $\boldsymbol{K}$ can be derived as a function of the statics matrix as follows.

$$\begin{aligned} \begin{bmatrix} \mathbf{F} \\ \mathbf{M} \end{bmatrix} &= \boldsymbol{K} \begin{bmatrix} \mathbf{\Delta X} \\ \mathbf{\Delta}\theta \end{bmatrix} = \mathbf{H}\mathbf{F}_a = \mathbf{H}\boldsymbol{K}_L\mathbf{\Delta L} \\ &= \mathbf{H}\boldsymbol{K}_L\mathbf{J}^{-1} \begin{bmatrix} \mathbf{\Delta X} \\ \mathbf{\Delta}\theta \end{bmatrix} = \mathbf{H}\boldsymbol{K}_L\mathbf{H}^T \begin{bmatrix} \mathbf{\Delta X} \\ \mathbf{\Delta}\theta \end{bmatrix} \\ \Rightarrow \quad & \mathbf{K} = \mathbf{H}\boldsymbol{K}_L\mathbf{H}^T \end{aligned} \tag{9}$$

where $\boldsymbol{K}_L$ is a 6×6 diagonal matrix with the individual link stiffnesses along the diagonal. The result in eq.(9) has the benefit that no matrix inversions are required to calculate the Cartesian stiffness at X, Y and Z coordinates, including coordinates where $\mathbf{H}$ is singular.

The static matrix of the Gantry-Tau was presented and described first in Hovland *et al.* (2007). However, the static matrix calculation presented in Hovland *et al.* (2007) has a significant drawback. The workspace of the Gantry-Tau is shown as a grid in YZ-plane and the static matrix is calculated for every cell of the grid. This method is faster than other known methods based on

numerical forward kinematics or Jacobian matrix but still computationally expensive. An extension of the method presented in Hovland *et al.* (2007) is presented in this paper. The extended method uses a geometric algebra and a functional dependency analysis to calculate the static matrix.

The elements of the matrix $\mathbf{H}$ are the X, Y and Z components of the vectors pointing from the actuator positions to the points A, B, C, D, E, F on the platform and X, Y and Z components of the cross products of these vectors and vectors pointed from the $\mathbf{TCP}$ to the points A, B, C, D, E, F on the platform, see Fig.3.

The vectors pointing from the actuator positions to the points A, B, C, D, E, F on the platform are given below

$$\begin{aligned} \mathbf{A} &= [A_x\ A_y\ A_z]^T \\ \mathbf{B} &= [B_x\ B_y\ B_z]^T \\ \mathbf{C} &= [C_x\ C_y\ C_z]^T \\ \mathbf{D} &= [D_x\ D_y\ D_z]^T \\ \mathbf{E} &= [E_x\ E_y\ E_z]^T \\ \mathbf{F} &= [F_x\ F_y\ F_z]^T \end{aligned} \tag{10}$$

$A_x, A_y, A_z, B_x, B_y, B_z, \cdots, F_x, F_y, F_z$ are the X-, Y- and Z-components of the normalised vectors pointing from the actuator positions to the points on the robot's platform, see Fig.3.

The 6×6 static matrix $\mathbf{H}$ is given below.

$$\mathbf{H} = \begin{pmatrix} A_x & \dots & F_x \\ A_y & \dots & F_y \\ A_z & \dots & F_z \\ (\mathbf{A} \times \mathbf{A_{TCP}})_x & \dots & (\mathbf{F} \times \mathbf{F_{TCP}})_x \\ (\mathbf{A} \times \mathbf{A_{TCP}})_y & \dots & (\mathbf{F} \times \mathbf{F_{TCP}})_y \\ (\mathbf{A} \times \mathbf{A_{TCP}})_z & \dots & (\mathbf{F} \times \mathbf{F_{TCP}})_z \end{pmatrix} \tag{11}$$

where $\mathbf{A_{TCP}} \dots \mathbf{F_{TCP}}$ are vectors pointed form $\mathbf{TCP}$ to the points on the platform.

According to the kinematic description presented in Murray *et al.* (2005), the vectors from the actuators to the points on the platform are:

$$\begin{aligned} \mathbf{A} &= [(a_x C + a_z S + dX_1)\ (a_y + dY_1)\ (a_z C - a_x S + dZ_1)]^T \\ \mathbf{B} &= [(b_x C + b_z S + dX_2)\ (b_y + dY_2)\ (b_z C - b_x S + dZ_2)]^T \\ \mathbf{C} &= [(c_x C + c_z S + dX_3)\ (c_y + dY_3)\ (c_z C - c_x S + dZ_3)]^T \\ \mathbf{D} &= [(d_x C + d_z S + dX_4)\ (d_y + dY_4)\ (d_z C - d_x S + dZ_4)]^T \\ \mathbf{E} &= [(e_x C + e_z S + dX_5)\ (e_y + dY_5)\ (e_z C - e_x S + dZ_5)]^T \\ \mathbf{F} &= [(f_x C + f_z S + dX_6)\ (f_y + dY_6)\ (f_z C - f_x S + dZ_6)]^T \end{aligned} \tag{12}$$

where $C = \cos\alpha$, $S = \sin\alpha$, X, Y, Z are the $\mathbf{TCP}$ coordinates. $dX_i = X - T_{ix}$, $dY_i = Y - T_{iy}$, $dZ_i = Z - T_{iz}$, where T_{ix}, T_{iy}, T_{iz} are the coordinates of actuator i for the given $\mathbf{TCP}$ position. Note, that T_{iy}, T_{iz} are constants and depend on support frame design parameters only, but T_{ix} is a function of the angle α. $[a_x a_y a_z]$, $[b_x b_y b_z]$, $[c_x c_y c_z]$, $[d_x d_y d_z]$, $[e_x e_y e_z]$, $[f_x f_y f_z]$ are the coordinates of the points A, B, C, D, E, F in the $\mathbf{TCP}$ coordinate frame.

The $\cos\alpha$ and $\sin\alpha$ equations are given below:

$$\cos\alpha = \frac{T_{3z} - Z}{\sqrt{L_{3m}^2 - (Y + M_y - T_{3y})^2} + \sqrt{M_x^2 + M_z^2}} \tag{13}$$

$$\sin\alpha = \sqrt{1 - \cos^2\alpha} \tag{14}$$

L_{3m} is the middle length of the triangular-mounted arm 3. M_x, M_y, M_z are coordinates of a midpoint M between the triangular link coordinates C and E on the platform, see Fig. 3.

YZ functional dependency is applied to find the elements of the static matrix $\mathbf{H}$.

Stage 1. In this stage all constants are found. The constants are coordinates of the points $A \dots F$ on the platform in the $\mathbf{TCP}$ coordinate frame, Y and Z coordinates of the actuators and link lengths. All these constants are the same for the different YZ coordinates of the $\mathbf{TCP}$.

Stage 2. In this stage Y coordinate is fixed and Z coordinate is variable. The upper limit of Z coordinate depends on the support frame parameter Q_1 and the lower limit is 0. In this paper a calculation algorithm for the first column of the static matrix is presented. The other 5 columns will be found in the same way.

Stage 2.1. According to eqs. (11-12)

$$H_{21} = a_y + Y - T_{1y} \tag{15}$$

where Y coordinate of the point A in the $\mathbf{TCP}$ coordinate frame a_y is a constant, Y coordinate of the actuator T_{1y} for the point A is a constant. Y coordinate of the $\mathbf{TCP}$ - Y is a constant for the fixed Y and variable Z $\mathbf{TCP}$ positions. The elements H_{2i} of row number 2 of the static matrix $\mathbf{H}$ will be found as a linear dependency of $\mathbf{TCP}$ Y coordinate.

Stage 2.2. According to eqs. (11-12)

$$H_{31} = a_z \cos\alpha - a_x \sin\alpha + Z - T_{1z} \tag{16}$$

where a_z, a_x, T_{1z} are constants for a fixed Y and a variable Z $\mathbf{TCP}$ coordinate. Equations for the angle α is rewritten for the variable Y and Z $\mathbf{TCP}$ coordinates.

$$\cos\alpha = \frac{T_{3z} - Z}{\sqrt{C_1' Y^2 + C_2' Y + C_3'}}$$

where C_1', C_2', C_3' are help constants and are found from eq. (13). For fixed Y an equation for $\cos\alpha$ is given below.

$$\cos\alpha = \frac{T_{3z} - Z}{\sqrt{C_1''}} \quad \sin\alpha = \sqrt{1 - \frac{(T_{3z} - Z)^2}{C_1''}} \tag{17}$$

According to eqs. (16-17) an equation for the element H_{31} is given below.

$$\begin{aligned} H_{31} &= a_z \frac{T_{3z} - Z}{\sqrt{C_1''}} - a_x \sqrt{1 - \frac{(T_{3z} - Z)^2}{C_1''}} + Z - T_{1z} \Rightarrow \\ H_{31} &= C_1''' + C_2''' Z + C_3''' \sqrt{C_4''' Z^2 + C_5''' Z + C_6'''} \end{aligned} \tag{18}$$

Stage 2.3. In this stage the element H_{11} of the static matrix $\mathbf{H}$ will be found. According to eqs. (11-12)

$$H_{11} = a_x \cos\alpha + a_z \sin\alpha + X - T_{1x} \tag{19}$$

where $X - T_{1x}$ will be found from previous stages.

$$X - T_{1x} = \sqrt{L_i^2 - (Y - T_{1y})^2 - (Z - T_{1z})^2} \quad (20)$$

$$X - T_{1x} = \sqrt{C_{10}'' Z^2 + C_{11}'' Z + C_{12}''} \quad (21)$$

where eq. (21) is a simplification of eq. (20) for a fixed Y and a variable Z **TCP** coordinates. According to eqs. (17) and (21) the element H_{11} of the static matrix $\mathbf{H}$ is given below.

$$H_{11} = C_{10}''' + C_{11}''' Z + C_{12}''' \sqrt{C_4''' Z^2 + C_5''' Z + C_6'''} + ... \\ ... \sqrt{C_{10}'' Z^2 + C_{11}'' Z + C_{12}''} \quad (22)$$

Note, that some constants for eq. (22) were found in Stage 2.2.

Stage 2.4. The element H_{41}, H_{51}, H_{61} of the static matrix $\mathbf{H}$ will be found in this stage. The elements are X, Y, Z coordinates of a vector cross product between a vector pointed from the **TCP** to the point A on the platform and a vector pointed from the actuator position to the point A on the platform.

The vector cross product related to the point A will be defined as given below.

$$H_{41} = (\mathbf{A_{TCP}} \times \mathbf{A})_x = (\mathbf{A_{TCP}}_y A_z - \mathbf{A_{TCP}}_z A_y) \quad (23)$$

$$H_{51} = (\mathbf{A_{TCP}} \times \mathbf{A})_y = (\mathbf{A_{TCP}}_z A_x - \mathbf{A_{TCP}}_x A_z) \quad (24)$$

$$H_{61} = (\mathbf{A_{TCP}} \times \mathbf{A})_z = (\mathbf{A_{TCP}}_x A_y - \mathbf{A_{TCP}}_y A_x) \quad (25)$$

where the vector's components in X, Y, Z directions are indicated by indexes $_x$,$_y$,$_z$. The vector pointing from the **TCP** to the point A on the platform ($\mathbf{A_{TCP}}$) is shown below.

$$\mathbf{A_{TCP}} = [(a_x \cos\alpha + a_z \sin\alpha) \;\; a_y \;\; (a_z \cos\alpha - a_x \sin\alpha)]^T \quad (26)$$

The elements H_{41}, H_{51}, H_{61} will be found from the previous stages as a multiplication of two functional dependencies or will be found in the second way. According to eqs. (11), (12) and (26) equations for the elements H_{41}, H_{51}, H_{61} of the static matrix $\mathbf{H}$ are given below.

$$\begin{aligned} H_{41} &= a_y(Z - T_{z1}) + (Y - T_{y1})(a_z \cos\alpha - a_x \sin\alpha) \\ H_{51} &= (Z - T_{z1})(a_x \cos\alpha + a_z \sin\alpha) - ... \\ &\quad ... - (X - T_{x1})(a_z \cos\alpha - a_x \sin\alpha) \\ H_{61} &= (Y - T_{y1})(a_x \cos\alpha + a_z \sin\alpha) - a_y(X - T_{x1}) \end{aligned}$$

The functional dependencies for H_{41}, H_{51}, H_{61} will be found according to eq. (17). The algorithm was presented in previous stages.

5 Dynamic Analysis

In this section a new method for calculating the frequency response of the Gantry-Tau based on the Laplace transform and a functional dependency of the static matrix and stiffness is presented.

In this paper some approximations and simplifications were assumed. The stiffness of the joint is much lower than the stiffness of the link. The link arm of Fig. 8 is simplified to the model

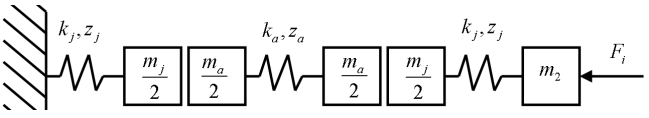

Figure 8: *Flexible link model.*

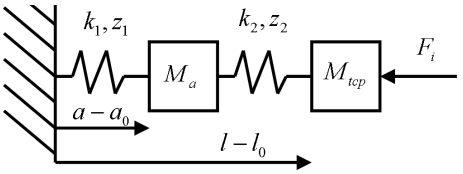

Figure 9: *Simplified flexible link model.*

in Fig. 9. This simplification is made to reduce the complexity of the equations. Note, however, that the presented methods would also be applicable to the larger model of Fig. 8 without major modifications. The flexible model of a single link in Fig. 8 assumes that the actuator is rigid and stationary. For an accurate modelling of a link a number of serially connected masses and springs can be used.

The parameters k_j and damper z_j represent the flexibility in the universal joint. The mass m_j is the total weight of the joint. In Fig. 8 only half of the joint mass is used, as it is assumed that one half of the joint is rigidly attached to the stationary actuator. The mass m_a is the total weight of the link between the two universal joints. The two halves of the link weight are lumped together with the joint masses. The parameters k_a and z_a represent the link flexibility. The parameter m_2 represent the platform weight.

In Fig. 9 the platform mass M_{TCP} equals the previous m_2 plus six halves of the joint masses, ie. $M_{TCP} = m_2 + 3m_j$. The mass M_a equals the sum of the masses of the two joint halves and the total weight of the link, ie. $M_a = m_a + m_j$. The new stiffness parameters in Fig. 9 are chosen the same ($k_1 = k_2$) and are calculated from the stiffness parameters of Fig. 8 such that the overall static stiffness is the same, ie.

$$\frac{1}{k_1} + \frac{1}{k_2} = \frac{2}{k_1} = \frac{2}{k_j} + \frac{1}{k_a} = \frac{2k_a + k_j}{k_a k_j} \quad (27)$$

$$k_1 = \frac{2k_a k_j}{2k_a + k_j} \quad (28)$$

Notice that $k_1 = k_j$ (the stiffness in the simplified model equals the joint stiffness) if $k_a >> k_j$. Isolating the dynamics for link i

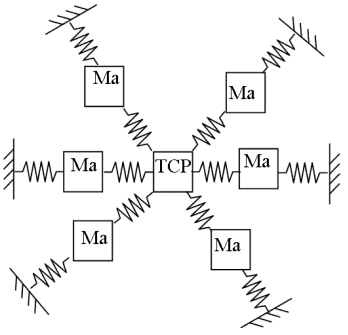

Figure 10: *Flexible model of 6-link PKM.*

and then the platform, the flexible equations of motion become

$$M_a\ddot{a}_i = -k_1 a_i - z_1\dot{a}_i + (l_i - a_i)k_2 + (\dot{l}_i - \dot{a}_i)z_2 \quad (29)$$

$$M_{TCP}\ddot{\boldsymbol{X}} = \boldsymbol{F} + \sum_j (a_j - l_j)k_2\boldsymbol{u}_j + \sum_j (\dot{a}_j - \dot{l}_j)z_2\boldsymbol{u}_j \quad (30)$$

$$I_{TCP}\ddot{\boldsymbol{\theta}} = \boldsymbol{M} + \sum_j (a_j - l_j)k_2(\boldsymbol{A}_j \times \boldsymbol{u}_j) + \sum_j (\dot{a}_j - \dot{l}_j)z_2(\boldsymbol{A}_j \times \boldsymbol{u}_j) \quad (31)$$

where $\boldsymbol{u}_j$ and $\boldsymbol{A}_j$ were introduced in eq.(6). By introducing the Laplace transform, the 18 equations above can be written on matrix form as follows.

$$\begin{bmatrix} A & -B \\ C & D \end{bmatrix} \begin{bmatrix} a_i \\ l_i \end{bmatrix} = \begin{bmatrix} \mathbf{0} \\ \boldsymbol{F} \\ \boldsymbol{M} \end{bmatrix} \quad (32)$$

where $\mathbf{0}$ is a 6×1 zero vector. The matrix elements A, B, C and D are functions of the Laplace transform, the masses and the flexibility parameters. For example,

$$A = \left(M_a s^2 + (z_1 + z_2)s + k_1 + k_2\right)\boldsymbol{I}_6 \quad (33)$$

$$B = (z_2 s + k_2)\boldsymbol{I}_6 \quad (34)$$

where $\boldsymbol{I}_6$ is a 6×6 identity matrix. In addition to the link masses, springs and dampers, the 6×6 sub-matrices C and D will also contain platform parameters, such as the platform weight and inertia. The Cartesian position vector $\boldsymbol{X}$ and the orientation vector $\boldsymbol{\theta}$ are replaced by a and l by using the Jacobian matrix.

Hence, the 12 unknown parameters a_i and l_i can be solved by inverting the matrix in eq. (32). If we know the direct link Jacobian matrix of the PKM, the Cartesian velocities can be calculated as follows.

$$\begin{bmatrix} \dot{\boldsymbol{X}} \\ \dot{\boldsymbol{\theta}} \end{bmatrix} = \boldsymbol{J}\dot{\boldsymbol{L}} \rightarrow s\boldsymbol{I}_6 \begin{bmatrix} \boldsymbol{X} \\ \boldsymbol{\theta} \end{bmatrix} = s\boldsymbol{I}_6\boldsymbol{J}\boldsymbol{L} \quad (35)$$

where $\boldsymbol{L} = [l_1, \cdots, l_6]^T$. The final transfer functions of the PKM from Cartesian forces or moments to Cartesian positions or orientation can then be derived from eqs.(32) and (35).

$$\frac{\boldsymbol{X}_i}{F_j}(s) = \frac{\boldsymbol{X}_i}{l_i}(s)\frac{l_i}{F_j}(s) \qquad \frac{\boldsymbol{\theta}_i}{M_j}(s) = \frac{\boldsymbol{\theta}_i}{l_i}(s)\frac{l_i}{M_j}(s) \quad (36)$$

6 First Resonance Frequency. The Laplace transform.

In this section a description of the method based on the Laplace transform to find the first resonance frequency is presented. The calculation algorithm to find the first resonance frequency of the PKM is also presented in this section. The Laplace transform was used before to find the Gantry-Tau first resonance frequency, see Hovland *et al.* (2007). The method presented in this section is an extension of the method in Hovland *et al.* (2007) and based on a functional dependency. The first resonance frequency calculation algorithm consists of a few stages.

Stage 1. All constants are found in this stage. Note, that constants are not ω, Y or Z dependent : M_{TCP}-the platform mass, M_a-the mass of the total weight of a link plus masses of the two joint halves, k_j-the joint stiffness, Sec_i- the section of the link (m^2), ε-Young's modulus, J_{pl}-an inertia matrix of the platform and z_1, z_2-damping ratio.

According to Hooke's law, the link stiffness are given below.

$$k_{1i} = \frac{2\varepsilon k_j Sec_i}{2\varepsilon Sec_i + k_j L_i}; \quad k_{2i} = K_{1i} \quad (37)$$

where L_i is the link length, $i = 1...6$, Sec_i is an area of the link section.

Stage 2. In this stage the equations for a_i through l_i will be found from eqs. (29) and (32).

$$a_i = BA^{-1}l_i \quad (38)$$

where A and B were found before, see eqs.(33 - 34).

Stage 3. A vector $L(s)$ as a function of the Laplace transform s will be found in this stage. Firstly, forces and moments in eqs. (30-31) will be divided by $M_{TCP}s^2$ and $I_{TCP}s^2$ to get the **TCP** 3-DOF position $\mathbf{X}$ and orientation $\boldsymbol{\theta}$ vectors.

$$U_i = \frac{(a_i - l_i)(k_2 + z_2 s)}{s^2 M_{TCP}}[H_{1i}\ \ H_{2i}\ \ H_{3i}]^T$$

$$V_i = \frac{(a_i - l_i)(k_2 + z_2 s)}{s^2}[H_{4i}\ \ H_{5i}\ \ H_{6i}]^T \quad (39)$$

where $i = 1...6$ according to the links, $H_{1i}, H_{2i}, H_{3i}, H_{4i}, H_{5i}, H_{6i}$ are elements of a static matrix $\mathbf{H}$, U is eq. (30) divided by $M_{TCP}s^2$ and V is eq. (31) divided by $I_{TCP}s^2$. Note, that elements $\mathbf{F}$ and $\mathbf{M}$ were not taken into account. According to eq. (38) the elements a_i will be replaced in eqs. (39).

$$U_i = l_i\frac{(BA^{-1} - 1)(k_2 + z_2 s)}{s^2 M_{TCP}}[H_{1i}\ \ H_{2i}\ \ H_{3i}]^T$$

$$V_i = l_i\frac{(BA^{-1} - 1)(k_2 + z_2 s)}{s^2}[H_{4i}\ \ H_{5i}\ \ H_{6i}]^T \quad (40)$$

Secondly, a vector $L(s) = [l_1...l_6]$ will be found from eq. (35). The Jacobian $\mathbf{J}$ is the transpose of the static matrix $\mathbf{H}$. A vector $L(s)$ consists of 6 unknown variables and the solution is a 6×6 matrix L_s

$$L_s = \mathbf{H}^T \begin{pmatrix} U_{h1} & U_{h2} & \ldots & U_{hi} \\ V_{h1} & V_{h2} & \ldots & V_{hi} \end{pmatrix} \quad (41)$$

where U_h and V_h are 3×6 matrixes.

$$U_{hi} = \frac{1}{s^2 M_{TCP}}[F_x\ \ F_y\ \ F_z]^T + U_i \quad (42)$$

$$V_{hi} = J_{pl}\frac{1}{s^2}[M_x\ \ M_y\ \ M_z]^T + V_i \quad (43)$$

Three elements (L_{s11}, L_{s12} and L_{s21}) of the matrix L_s are given

below. Other 33 elements will be found in the same way.

$$L_{s11} = \frac{H_{11}}{C_3} + l_1(-1 + C_1(H_{11}^2 + H_{21}^2 + H_{31}^2)) + ... \\ ... + C_2\left(\frac{H_{41}^2}{J_{pl11}} + \frac{H_{51}^2}{J_{pl22}} + \frac{H_{61}^2}{J_{pl33}}\right) \quad (44)$$

$$L_{s12} = \frac{H_{12}}{C_3} + l_2C_1(H_{11}H_{12} + H_{21}H_{22} + H_{31}H_{32}) + ... \\ ... + C_2\left(\frac{H_{41}H_{42}}{J_{pl11}} + \frac{H_{51}H_{52}}{J_{pl22}} + \frac{H_{61}H_{62}}{J_{pl33}}\right) \quad (45)$$

$$L_{s21} = \frac{H_{11}}{C_3} + l_1C_1(H_{11}H_{12} + H_{21}H_{22} + H_{31}H_{32}) + ... \\ ... + C_2\left(\frac{H_{41}H_{42}}{J_{pl11}} + \frac{H_{51}H_{52}}{J_{pl22}} + \frac{H_{61}H_{62}}{J_{pl33}}\right) \quad (46)$$

where C_1 and C_2 are help variables and are given below.

$$C_1 = (BA^{-1} - 1)\frac{k_2 + z_2 s}{s^2 M_{TCP}} \\ = -\frac{M_a z_2 s^3 + (M_a k_2 + z_1 z_2)s^2 + (z_1 k_2 + k_1 z_2)s + k_1 k_2}{M_{TCP}(M_a s^4 + (z_1 + z_2)s^3 + (k_1 + k_2)s^2)}$$

$$C_2 = (BA^{-1} - 1)\frac{k_2 + z_2 s}{s^2} = C_1 M_{TCP}$$

$$C_3 = s^2 M_{TCP}$$

According to eq. (46),

$$-\frac{H_{11}}{C_3} = l_1C_1(H_{11}H_{12} + H_{21}H_{22} + H_{31}H_{32}) + ... \\ ... + C_2\left(\frac{H_{41}H_{42}}{J_{pl11}} + \frac{H_{51}H_{52}}{J_{pl22}} + \frac{H_{61}H_{62}}{J_{pl33}}\right) \Rightarrow \quad (47)$$

$$-\frac{H_{1i}^T}{C_3} = \mathbf{S} * l_i \quad \Rightarrow \quad L(s) = -\frac{\mathbf{S}^{-1}H_{1i}^T}{C_3} \quad (48)$$

where $\mathbf{S}$ is a 6×6 matrix and l_i, H_{1i} are 6×1 vectors. The elements of $\mathbf{S}$ matrix are the elements of L_s matrix without $\frac{H_{1i}}{C_3}$ and divided by l_i. $\mathbf{S}$ is found from all 36 elements of L_s. l_i is a function of the Laplace transform. H_{1i} is a vector with elements equal to the elements of the first row of the static matrix $\mathbf{H}$.

Stage 4. The Cartesian **TCP** position vector as a function of the Laplace transform s will be found in this stage and an equation is given below.

$$X(s) = (\mathbf{H^{-1}})^T L(s) \quad (49)$$

where $L(s) = [l_1, l_2, ..., l_6]$.

Stage 5. The first resonance frequency will be found in this stage as the first maximum of the amplitude response. The equation is given below.

$$Amp = |X(j\omega)| \quad (50)$$

The Laplace transform s in eq. (50) is replaced by $j\omega$, where j is the complex unity and ω a frequency. The first resonance frequency is found by a search algorithm using the amplitude response.

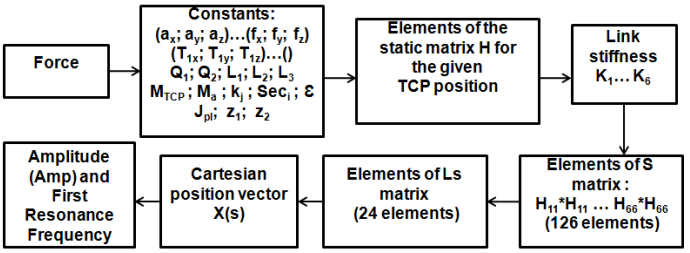

Figure 11: *The flowchart of the first resonance frequency calculation algorithm.*

A flowchart of the first resonance frequency calculation algorithm is shown in Fig. 11. The YZ functional dependency is applied to find the elements of static matrix $\mathbf{H}$, see section 4. Also, the YZ functional dependency is used to find the elements of matrix S, see eq. 48. The elements of the matrix $\mathbf{S}$ consist of two parts ω dependent C_1, C_2, see eqs. 47 and 48, and YZ dependent elements of the static matrix $\mathbf{H}$. The number of calculations will be reduced because the differences between the elements S_{12} and S_{21} are ω dependent elements C_1 and C_2. YZ dependent parts will be found once for the elements S_{12} and S_{21} and ω dependent parts will be added into account after that.

When all YZ dependent parts of the matrix $\mathbf{S}$ are found, the ω dependency is taken into account. Note, that elements C_1, C_2 of the matrix $\mathbf{S}$ have constant parts as coefficients before the Laplace transform s. The matrix $\mathbf{S}$ will be recalculated for the different frequencies ω without recalculating the YZ dependent part of the equations. In conclusion, there are two functional dependencies in the first resonance frequency calculation algorithm. Both of them will be found separately. Firstly, YZ dependent elements of the $\mathbf{S}$ matrix will be found. Secondly, ω dependent elements of matrix $\mathbf{S}$ can be found, because YZ dependent elements are independent of ω.

7 Combined Workspace and First Resonance Frequency Optimisation Problem

An optimal design for the Gantry-Tau (and other PKMs) is difficult to find manually. In this section an optimisation scheme based on the geometric descriptions of the workspace and a functional dependency of the first resonance frequency is presented. Two different scenarios are tested. The first optimisation problem is expressed as

$$\max\ k_{w1} * V_R(Q_1, Q_2, L_1, L_2, L_3) + ... \\ ... + k_{w2} * \gamma(Q_1, Q_2, L_1, L_2, L_3) \\ \text{subject to} \\ Q_1 > 0 \quad Q_2 > 0 \quad L_1 > 0 \quad L_2 > 0 \quad L_3 > 0$$

where k_{w1} and k_{w2} are weight parameters. A user must specify these constants depending on the weighting of workspace vs. stiffness. V_R is the total reachable workspace volume, γ is the minimum first resonance frequency. L_1, L_2, L_3 are the arm lengths. Q_1, Q_2 are the support frame parameters.

The second optimisation problem is defined as follows:

$$\max V_R(Q_1, Q_2, L_1, L_2, L_3)$$
$$\text{subject to}$$
$$Q_1 > 0 \;\; Q_2 > 0 \;\; \gamma > 48 \;\; L_1 > 0 \;\; L_2 > 0 \;\; L_3 > 0$$

where $\gamma = 48Hz$ is an example of a user specified minimum first resonance frequency level. This approach may be more suitable for optimisation in practice because the method maximises the total workspace while keeping the minimum first resonance frequency level above $48Hz$.

The total workspace volume V_R as a function of the two support frame design parameters Q_1, Q_2 and the individual arm lengths L_1, L_2, L_3 is maximised while maximising the minimum first resonance frequency. Without including the workspace into the first resonance frequency or the first resonance frequency into the workspace optimisation, it would not be possible to simultaneously optimise both the support frame parameters Q_1, Q_2 and the link lengths L_1, L_2, L_3 as these would all go to infinity. The optimisation results are presented in section 8.

8 Results

Each of the 12 universal joints has a weight $1.0kg$ and a stiffness 50 N/μm. The stiffnesses of the support frame and the actuators are assumed infinite. The links have weight $1.0kg$. The platform weight is $5kg$ and the inertia matrix I_{TCP} is a diagonal matrix with elements 0.06, 0.02 and 0.07.

The final optimisation design parameters of the Gantry-Tau were found using the $lsqnonlin$ function in MatLab. According to the weighting coefficients k_{w1} and k_{w2}, the optimisation problem has three solutions. A condition of the first solution is $k_{w1} < k_{w2}$ and the reachable workspace has a higher priority level than the first resonance frequency. The second solution has equal weights. The third solution prioritises the first resonance frequency. The solution's results are given as follows.

$$1: Q_1 = 0.4352 \;\; Q_2 = 0.9726 \;\; V_R = 3.8394$$
$$L_1 = 0.9782 \;\; L_2 = 0.9453 \;\; L_3 = 0.9417 \;\; \gamma = 45.3992$$

$$2: Q_1 = 0.4760 \;\; Q_2 = 1.0219 \;\; V_R = 3.7572$$
$$L_1 = 0.9432 \;\; L_2 = 0.9375 \;\; L_3 = 0.9411 \;\; \gamma = 46.5643$$

$$3: Q_1 = 0.5235 \;\; Q_2 = 1.0415 \;\; V_R = 3.6035$$
$$L_1 = 0.9581 \;\; L_2 = 0.9456 \;\; L_3 = 0.9512 \;\; \gamma = 48.7600$$

The results of the optimisation with a constrained minimum first resonance frequency level of $\gamma = 48Hz$ are given below. The design parameters were found using the $fmincon$ function in MatLab.

$$Q_1 = 0.5155 \;\; Q_2 = 1.0212 \;\; V_R = 3.6999$$
$$L_1 = 0.9482 \;\; L_2 = 0.9514 \;\; L_3 = 0.9467 \;\; \gamma = 47.9799$$

These results would have been difficult to obtain by a manual design, as all the link lengths are different and Q_2 is different from $2Q_1$ which has been a typical manual design choice of the Gantry-Tau in the past. In addition, acceptable first resonance frequency needs short arm lengths while the support frame is fixed, and an increase of the workspace volume requires long arm lengths. The required installation space of the Gantry-Tau equals $2Q_1Q_2 = 1.05m^3$ for the optimised design. Hence, the total workspace to installation space ratio for the optimised design is $V_{installation} = 3.5228$ which is large compared to most other PKMs which typically have a ratio of less than one.

9 Conclusions

In this paper an extension of the method, see Hovland *et al.* (2007), for calculating the frequency response of the triangular-link version of the Gantry-Tau has been developed. The method considers flexible links and universal joints and based on a functional dependency of the elements of the static matrix $\mathbf{H}$ and the Cartesian position vector $\mathbf{X}$. The model allows PKM resonance maps such as in Fig. 12 to be generated in very short time compared to FEM software packages. Table 1 shows the compu-

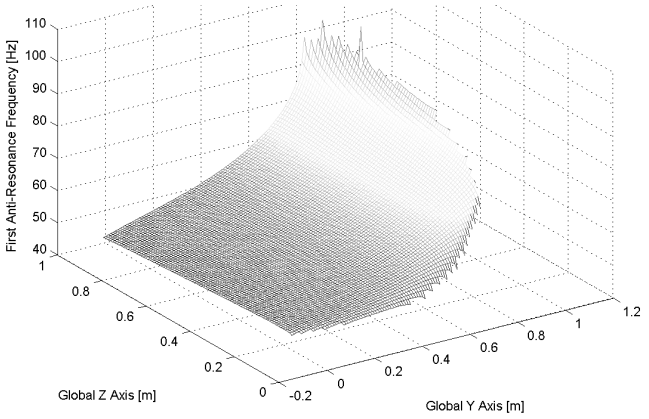

Figure 12: *First resonance frequency as function of the Y and Z coordinates at $X = 1.0$.*

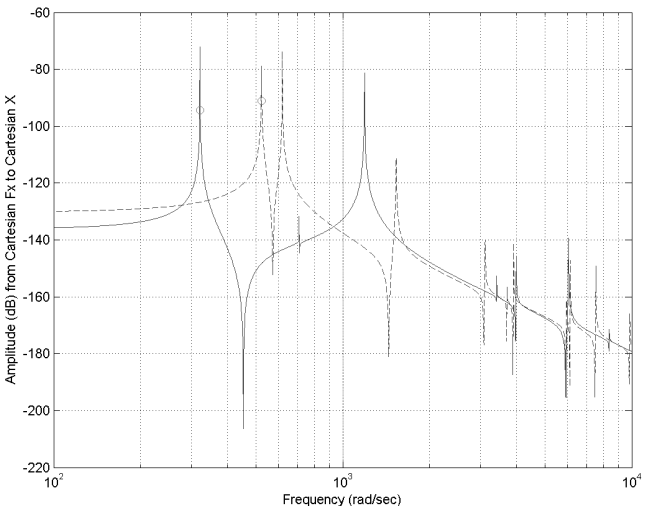

Figure 13: *Example of frequency response curves for the fixed-length version of the Gantry-Tau.*

Method	Time
Finite Element Method	5600
Method in Hovland *et al.* (2007)	$5-7$
Functional Dependency	1

Table 1: First resonance frequency computation time for three different methods.

tational requirements for the three different approaches on the triangular version of the 3-DOF Gantry-Tau PKM. The first resonance frequency calculation covers 70% of the entire workspace of the PKM. The method based on the functional dependency is 6500 times faster than the Finite Element Method. The computational time has been normalized to 1 for the third approach.

Fig. 13 shows two examples of the frequency response curves that are generated by the methods in Section 6. The solid curve shows the amplitude response from a Cartesian force in the X-direction to Cartesian position in the X-direction at $X = 1.0$, $Y = 0.0$ and $Z = 0.5$. The dotted curve shows the same response at $X = 1.0$, $Y = 0.8$ and $Z = 0.5$. The first resonance frequency occurs at 322 rad/sec or 51.2 Hz and 525 rad/sec or 83.6 Hz, respectively, for the two selected locations.

A map of the first resonance frequency as a function of the Y and Z coordinates for the Gantry-Tau is shown in Fig. 12. The frequency response data generated by the new method presented in this paper have been verified against calculations from a FE software package (Strand7). For a set of 10 locations in the workspace of the Gantry-Tau, the method in this paper generates the same results as the FE package and the method is also significantly faster. The maps in Fig. 12 can be generated approximately in the same time as it takes to set up and calculate one resonance frequency in a FE package.

Because of the significant computational benefits of the geometric approach and the method based on a functional dependency of elements, these methods are far better suited for inclusion in a design optimisation framework compared to discretisation, analytical or based on inverse kinematic approaches. The optimised design presented in this paper was obtained in less than 85 hours on a standard desktop computer using Matlab's Optimisation Toolbox.

The results in this paper show that it is possible to optimise the kinematic design of the Gantry-Tau PKM to achieve the first resonance frequency equal to $48\ Hz$ while maximising the reachable workspace.

Future extensions of the work presented in this paper will introduce performance criteria such as the Cartesian stiffness, singularities and collisions into the design optimisation.

References

Angeles, J., 1985, "On the Numerical Solution of the Inverse Kinematics Problem", *Int. J. Robotics Res.*, pp. 21-37, Vol. 4, 1985(2).

Bonev, I.A., Ryu, J., 2001, "A Geometrical Method for Computing the Constant-Orientation Workspace of 6-PRRS Parallel Manipulator", *Mechanism and Machine Theory*, pp. 1, Vol. 36, 2001(1).

Brogårdh, T., Hanssen, S., Hovland, G., 2005, "Application-Oriented Development of Parallel Kinematic Manipulators with Large Workspace", *Proc. 2nd Intl. Coll. of the Collaborative Research Center 562:Robotic Systems for Handling and Assembly*, pp. 153-170, Braunschweig, Germany, May, 2005.

Brogårdh, T., 2000, "Design of high performance parallel arm robots for industrial applications", *Proc. of the Symp. Commemorating the Legacy, Works, and Life of Sir Robert Stawell Ball Upon the 100th Anniversary of A Treatise on the Theory on The Screws*, University of Cambridge, Trinity College, 2000.

Chablat, D., Wenger, P., 2003, "Architecture Optimization of 3-DOF Translational Parallel Mechanism for Machining Applications , the Orthoglide", *IEEE Transactions on Robotics and Automat.*, pp. 403-410, Vol. 19, 2003(3).

Chen, J.S., Hsu, W.Y., 2006, "Dynamic and Compliant Characteristics of a Cartesian-Guided Tripod Machine", *Journal of Manufacturing Science and Engineering*, Vol. 128, pp. 494-502, 2006.

Clavel, R., 1988, "DELTA, a fast robot with parallel geometry", *Intl. Symp. on Industrial Robots*, pp. 91-100, Lausanne, Switzerland, 1988.

Dashy, A. K., Yeoy, S.H., Yangz, G., Chery, I. H., 2002, "Workspace Analysis and Singularity Representation of Three-Legged Parallel Manipulators", *Proc. 7th Intl. Conf. in Control, Automat., Robotics And Vision*, pp. 962-967, Singapore, 2002.

Fattah, A., Angeles, J., Misra, A.K., 1995, "Dynamics of a 3-DOF Spatial Parallel Manipulator with Flexible Links", *Proc. of the 1995 International Conference on Robotics and Automation*, pp.627-632, 1995.

Goldenberg, A. A., Benhahib, B., Fenton, R. G., 1985, "A Complete Generalized Solution to the Inverse Kinematics of Robots", *IEEE Journal Robotics Automat.*, pp. 14-20, Vol. 1, 1985(1).

Gosselin, C., 2007, "Determination of the Workspace of 6-DOF Parallel Manipulators", *ASME J. Mech. Des.*, pp. 331-336, Vol. 112, 1990.

Gough, V. E., 1957, "Contribution to Discussion to Papers on Research in Automobile Stability and Control and in Tire Perfomance", *Proc. Auto. Div. Institute of Mechanical Engineers*, pp. 392-394, 1956-1957.

Hovland, G., Choux, M., Murray, M., Brogårdh, T., 2007, "Benchmark of the 3-DOF Gantry-Tau Parallel Kinematic Machine", *IEEE Intl. Conf. on Robotics and Automat.*, pp. 535-542, Roma, Italy, 2007.

G. Hovland, M. Choux, M. Murray, I. Tyapin and T. Brogrdh, "The Gantry-Tau Summary of Latest Development at ABB, University of Agder and University of Queensland", Invited Paper, *Proc. of the 3rd Intl. Colloquium: Robotic Systems for Handling and Assembly, the Collaborative Research Centre SFB 562*, Braunschweig, Germany, April 2008.

Johannesson, S., Berbyuk, V., Brogårdh, T., 2004, "A New Three Degrees of Freedom Parallel Manipulator", *Proc. 4th Chemnitz Parallel Kinematics Seminar*, pp. 731-734, Chemnitz, Germany, 2004.

Kim, D.I., Chung, W.K., Youm, Y., 1997, "Geometrical Approach for the Workspace of 6-DOF Parallel Manipulators", *Intl. Conf. on Robotics and Automat.*, pp. 2986-2991, Albuquerque, 1997.

Liu, X. J., Wang, J. S., Gao, F., 2000, "On the Optimum Design of Planar 3-DOF Parallel Manipulators with Respect to the Workspace", *Intl. Conf. on Robotics and Automat.*, pp. 4122-4127, San Francisco, 2000.

Merlet, J.-P., 2000, "Parallel Robots", *Kluwer Academic Publisher, Solid Mechanics and its Applications*, p 355, Vol. 74, Dordrecht, Boston, 2000.

Monsarrat, B., Gosselin, C., 2003, "Workspace Analysis and Optimal Design of a 3-Leg 6-DOF parallel Platform Mechanism", *Transactions on Robotics and Automat.*, pp. 954-966, Vol. 19, 2003(6).

Murray, M., Hovland, H., Brogårdh, T., 2006, "Collision-Free Workspace Design of the 5-Axis Gantry-Tau Parallel Kinematic Machine", *Proc. of the 2006 IEEE/RSJ Intl. Conf. on Intelligent Robots and Systems*, pp. 2150-2155, Beijing, 2006.

Pierrot, F., Uchiyama, M., Dauchez, P., Fournier, A., 1992, "A New Design of a 6-DOF Parallel Robot", *Proc. 23rd Intl. Symp. on Industrial Robots*, pp. 771-776, 1992.

Stewart, D., 1965, "A Platform with Six Degrees of Freedom", *UK Institution of Mechanical Engineers Proceedings*, Vol. 180, 1965(15).

Tyapin, I., Hovland, G., Brogårdh, T., 2006, "Kinematic Optimisation of the Gantry-Tau Parallel Kinematic Manipulator with Respect to its Workspace", *Australasian Conf. on Robotics and Automat.*, Auckland, New Zealand, 2006.

Tyapin, I., Hovland, G., Brogårdh, T., 2007, "A Fully Geometric Approach for the Workspace Area of the Gantry-Tau Parallel Kinematic Manipulator", *Proc. of the 13th IASTED Intl. Conf. on Robotics and Applications*, pp. 437-444, Wurzburg, Germany, 2007.

Uchiyama, M., Iimura, K. I., Pierrot, F., Dauchez, P., Unno, K., Toyama, O., 1990, "A New Design of a Very Fast 6-DOF Parallel Robot", *Journal of Robotics and Mechatronics*, pp. 308-315, 1990(2).

Williams, I., Hovland, G., Brogårdh, T., 2006, "Kinematic Error Calibration of the Gantry-Tau Parallel Manipulator", *IEEE Intl. Conf. on Robotics and Automat*, pp. 4199-4204, Orlando, May, 2006.

Xi, F., Sinatra, R., Han, W., 2001, "Effect of Leg Inertia on Dynamics of Sliding-Leg Hexapods", *Journal of Dynamic Systems, Measurement and Control*, Vol. 123, pp. 265-271, 2001.

Zhou, Z., Xi, F., Mechefske, C. K., 2006, "Modeling of a Fully Flexible 3PRS Manipulator for Vibration Analysis", *Journal of Mechanical Design*, Vol. 128, pp. 403-412, 2006.